Anchoring of Gold Nanoparticles on Graphene Oxide and Noncovalent Interactions with Porphyrinoids

Suzana M. Andrade,*[a] Carlos J. Bueno-Alejo,[a] Vanda V. Serra,[a, b] João M. M. Rodrigues,[b] Maria G. P. M. S. Neves,[b] Ana S. Viana,[c] and Sílvia M. B. Costa[a]

Abstract: The interaction of tetrasulfonated aluminium phthalocyanine (AlPcS4) and *meso*-tetraarylporphyrin mono-substituted with poly-L-lysine (MM-PLL), with graphene oxide (GO) is studied in aqueous solution using spectroscopic and microscopic techniques. The study is also performed in the presence of gold nanoparticles (AuNP) grown on the surface of GO using a sonochemical method. The strong quenching of the porphyrin luminescence demonstrates the important interactions between the excited state of the molecule with GO which are absent in the case of the phthalo-cyanine. However, in the presence of AuNP@GO hybrid a concomitant increase of the phthalocyanine fluorescence intensity takes place together with a decrease of the fluorescence lifetimes involving a surface plasmon coupling effect. The latter is overcome in case of MM-PLL due to stronger interactions with GO, and is corroborated for deposited samples using fluorescence lifetime imaging microscopy (FLIM). These new nanostructures are thus expected to have selective sensing abilities.

Introduction

Due to remarkable electronic and optical properties combined with outstanding mechanical strength and impressive surface area, single-layer two-dimensional graphene structure opens up new opportunities.[1] The design of composite materials with tailored properties has thus gained considerable attention for a wide range of applications from energy conversion devices to sensing.[2]

Pristine graphene sheets are hydrophobic in nature, and as a result of strong van der Waals forces, graphene sheets tend to stack thus preventing its processing and purification, important requisites for integration into devices. Although covalent or noncovalent functionalization of graphene has been consid-ered to be important to graphene solubility and processing, the possibility to combine graphene superior properties and those of the functionalizing material has driven special inter-est.[3] Chemical exfoliation of graphene to produce graphene oxide (GO) is a convenient route to synthesize large batches of the single-layer material, which readily suspends in polar sol-vents. Moreover, oxygen groups introduced along with struc-tural defects provide a negatively charged surface, where van der Waals and electrostatic forces can be used to complex op-positely charged electron donors and/or acceptors.[4]

In this regard, porphyrinoids (e.g., porphyrins and phthalo-cyanines) are quite suitable choices. Porphyrinoids are elec-tronically and steriochemically tunable by chemical modifica-tion of the central metal ion and of the peripheral groups They contain an extensively conjugated 2D π-system, are adequate for synthetic light harvesting and for efficient electron transfer (ET) and, therefore, their conjugation with graphene has been explored for photoactive assemblies.[5]

Graphene and derivatives are also effective substrates for the dispersion of metal nanoparticles (MNPs),[6] and various ap-proaches for their preparation have been proposed.[7] MNPs can act as electron donors or acceptors in photocatalysis reac-tions or they can produce highly localized heat during the rapid relaxation process that can be used for photothermal therapies, for example, in treating cancer.[8] MNPs that have surface plasmon resonance bands (SPRBs) are of particular in-terest because they can have an antenna effect and increase the absorption and/or emission of fluorescent molecules by orders of magnitude. The subjacent phenomenon of fluores-cence enhancement promoted by a metal surface plasmon in the near-field (MEF) has found considerable interest in recent

[a] Dr. S. M. Andrade, Dr. C. J. Bueno-Alejo,+ Dr. V. V. Serra, Prof. S. M. B. Costa
Centro de Química Estrutural, Instituto Superior Técnico
Universidade de Lisboa
Av. Rovisco Pais, 1049-001 Lisboa (Portugal)
E-mail: suzana.andrade@tecnico.ulisboa.pt

[b] Dr. V. V. Serra, J. M. M. Rodrigues, Prof. M. G. P. M. S. Neves
Departamento de Química & QOPNA
Universidade de Aveiro
Campus Universitário de Santiago, 3810-193 Aveiro (Portugal)

[c] Dr. A. S. Viana
Centro de Química e Bioquímica, Faculdade de Ciências
Universidade de Lisboa
Ed. C8, Campo Grande, 1749-016 Lisboa (Portugal)

years due to the opportunity to tune the brightness and photostability of fluorophores and the applications in materials science, electronics, and biomedicine.[9] MEF is characterized by an increase in the fluorescence intensity and a decrease in fluorescence lifetime of a fluorophore in the vicinity of the plasmonic nanostructure. The metal effect is highly dependent on the chemical nature of the metal, the particle shape and size,[10] the distance and the orientation of the chromophore with respect to the particle,[11] their spectral overlap,[12] and the environment in which the fluorescence process takes place (e.g., supported on surfaces, in water).[13]

Although there have been recent studies involving noncovalent interactions of porphyrinoids with graphene[14] (or graphene oxide),[15] the combination of these hybrids with metal nanoparticles is still scarcely explored.[16] The aim of this study is, therefore, to combine through noncovalent interactions fluorescent planar molecules with graphene-based material decorated with metal nanoparticles and investigate the conditions under which photoinduced electron transfer or MEF are promoted.

Towards these goals, we have synthesized hybrid materials of gold nanoparticles and GO and followed their interaction with tetrasulfonated aluminium phthalocyanine (AlPcS4) and a tetraarylporphyrin monosubstituted in one of the phenyl groups with a poly-L-lysine chain (MM-PLL), Scheme 1. The mo-
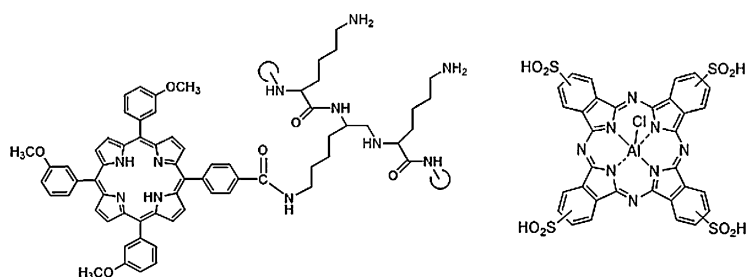
Scheme 1. Molecular structures of MM-PLL (left) and of AlPcS4 (right).

tivation for the synthesis of the latter came from the fact that PLL has a high density of partially protonated primary amines which contributes to the solubilization in water and potentiates interactions with oxygenated groups in GO. Due to its flexible backbone, PLL was found suitable to disperse individual SWCNT and MWCNT in aqueous solution.[17] In turn, AlPcS4 has been successfully employed in many donor–acceptor systems, as previously reported.[18] The fluorescence of AlPcS4 was shown to be enhanced in the presence of gold nanostructures and the effect could be tuned by varying metal–molecule distances.[19] In addition, AlPcS4-gold nanorods conjugates were reported to exhibit a more effective photodynamic effect as compared to the phthalocyanine alone.[20] The ground-state interaction as well as the mechanism of excited-state deactivation of the two porphyrinoids on GO and AuNP@GO hybrid surfaces were probed. Results obtained for the systems in solution were compared with those obtained using fluorescence lifetime imaging microscopy (FLIM)[21] of deposited films.

Results and Discussion

Characterization of GO and AuNP@GO

GO was prepared by a variation of the Hummers method (see details in Experimental Section). In this method, the strong oxidation process helps to exfoliate the graphite and to avoid the graphene layers coming together again. The characterization of the material was made using different spectroscopic techniques: XPS, Raman, UV/Vis (Figures S1 and S2, Supporting Information). The zeta potential (ζ) of aqueous suspensions of GO was measured at pH 6.0 confirming the GO substrate presents a higher density of oxygen functionalities at its surface ($\zeta \approx -52$ mV).

Microscopic studies were also carried out. The morphology of GO sample generated from aqueous solution was observed by transmission electron microscopy (TEM) and atomic force microscopy (AFM), Figure 1. Large silk-like graphene nanosheets were observed with crumpled or wrinkled structures, indicating the presence of few-layer graphene, Figure 1 A.

The lateral dimensions of GO sheets range from submicrometer to one micrometer, Figure 1 B. A typical cross-section picture, Figure 1 C, indicates a narrow height distribution around 1.2 ± 0.1 nm suggesting the formation of mostly single-layer GO sheet in agreement with literature data.[22] The introduction of functional groups on both sheet surfaces leads to a thickness that is greater than the theoretical value of 0.34 nm. Besides, a thin layer of water should be present in all AFM experiments conducted at ambient conditions which can further contribute to that greater thickness.

In the next stage, we proceeded to attach AuNP to the surface of the material. The sonolysis method reported in literature by Vinodgopal et al. in 2010[23] was used with some variations. Sonolysis of dispersed Ar, N_2, or O_2 in aqueous solutions result in acoustic cavitation. The growth and violent collapse of microbubbles during cavitation leads to high temperature conditions within bubbles able to generate highly reactive radicals like H• and OH• from water homolysis. These radicals are unlikely to reach the target molecules in solution due
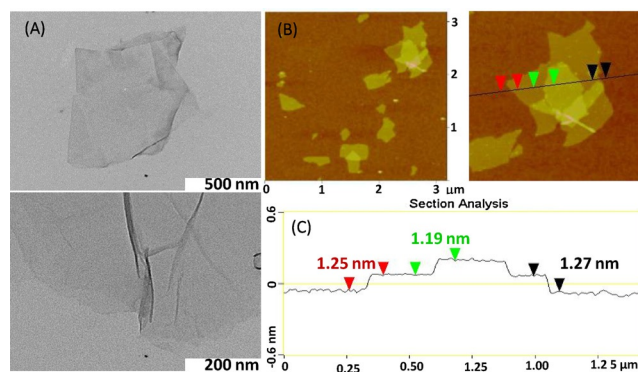
Figure 1. TEM images (A), AFM (B) images, and height analysis (C) of a GO sample.

to rapid recombination or reaction within the bubbles. If organic molecules are present (e.g., tetraethylene glycol), they will act as a scavenger for the oxidative radicals generated providing the reduction of the Au salt.

To confirm the presence of the AuNP on the surface of the GO we registered the absorption spectrum of the suspension and used TEM and AFM microscopies. A representative TEM image is depicted in Figure 2A, from which it is possible to see
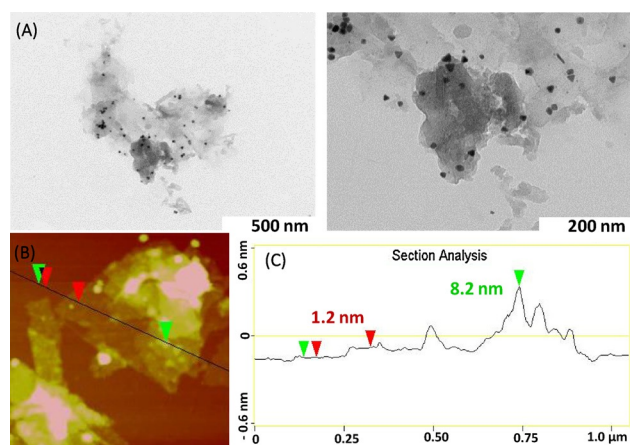
Figure 2. TEM images (A), AFM (B) image and height analysis (C) of AuNP@GO samples.

that AuNP distribute all over the surface of GO with no apparent tendency for NP aggregation, corroborated by UV/Vis spectra where no broad redshifted plasmon band was observed. Importantly, AuNP are formed almost exclusively on the surface of GO (no stand-alone NP were observed outside the sheet, see also Figure S3, Supporting Information). Nonetheless, there seems to be a certain heterogeneity regarding the NP shape (mostly spheres, rods, and triangles can be obtained). Tapping-mode AFM of the hybrids, Figure 2B, also confirms AuNPs adhered to GO surface. From the height analysis of these images, we can estimate the dimensions of the NPs. Average sizes around 10 nm were obtained in good agreement with TEM results.

These values are within the range of sizes obtained using other in situ methods with distinct reducing/capping agents, for example, sodium citrate, were reported to have an average size of 20 nm,[7a] and those prepared using glycine were significantly smaller (ca. 6 nm).[24]

In Figure S4 (Supporting Information), it is shown the absorption spectra of the samples obtained at different reaction times which reflect the growth of the surface plasmon resonance band around 545 nm. This band is slightly redshifted compared to that of individual AuNP free in solution which is due to the higher dielectric environment of the GO surface.[25] The ζ-potential of AuNP@GO aqueous suspension ($\zeta \approx -57$ mV) is slightly more negative than that of GO.

In an attempt to optimize the synthesis of the hybrid material and maximize the amount of supported AuNP on GO, we compared two methods for the same amount of Au salt addi-

tion: Method 1—addition of increasing amounts of Au salt; Method 2—addition of a constant amount of Au salt sequentially and sonication after each addition (Figure S5, Supporting Information). From TEM images and size distribution analysis (made using ImageJ[26]) it is clear that the two methods lead to similar hybrids in terms of average size and distribution of AuNP on GO sheets, Figure 3. Therefore, Method 1 was chosen since it involved fewer preparation steps.
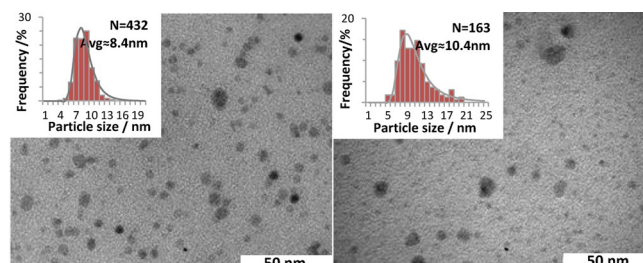
Figure 3. TEM images and size distribution (insets) of AuNP deposited on GO obtained using method 1 (left) and method 2 (right) for additions of increasing amount of Au salt (see text for explanation).

Interactions between GO and porphyrinoids

Two different porphyrinoids, AlPcS4 and MM-PLL were employed to interact with GO. AlPcS4 is a widely used phthalocyanine, which does not form aggregates in aqueous solution up to a concentration of 10^{-4} M.[18] Stacking of AlPcS4 molecules is prevented due to the fact that aluminum coordinates axially with chloride, which slightly distorts the aromatic structure. The synthesized porphyrin is only sparingly water soluble. To get a better insight into the aggregation properties of the synthesized porphyrin, a stock solution of the porphyrin was prepared in DMSO, and a few microliters were added to the final aqueous solution which corresponds to less than 1% of DMSO. Taking a more detailed look, we see that the electronic spectrum obtained for the porphyrin in each solvent is different, Figure 4A. The spectrum in DMSO shows the common intense Soret band around 420 nm corresponding to the allowed S_0 to S_2 transition; and four less-intense Q-bands at lower energies with peaks matching those reported for other *meso*-substituted porphyrins.[27] The spectral broadening (to the red and to the blue) and the hypochromicity found in aqueous solution as compared to DMSO, is indicative of the formation of J- and
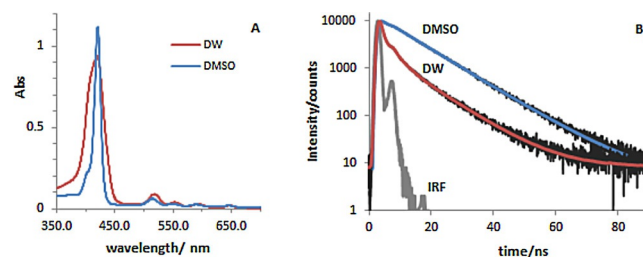
Figure 4. (A) Absorption spectra and (B) fluorescence decays of MM-PLL obtained in neat DMSO and in distilled water (DW) with 1% DMSO (IRF = instrument response function).

H-aggregates as deduced from excitonic theory.[28] Nonspecific aggregates were promoted in the case of another *meta*-methoxyl porphyrin functionalized with a dipeptide glycilglycine in water. The aggregates are stabilized due to hydrophobic interactions and to noncovalent intermolecular H-bonds.[29] The fact that excitation spectra obtained did not match that of absorption in water which did not occurred in DMSO further corroborates that aggregates are formed in water. As a consequence, the monoexponential fluorescence decay obtained in pure DMSO ($\tau_f \approx 11$ ns, upon excitation at 445 nm and collected at 650 nm) changes to a very complex decay in water where good fitting are obtained only by a triexponential function, Figure 4B. In the case of the latter, there is only a minor contribution from a long component ($\tau_f \approx 10$ ns, 8%) which can be assigned to the monomer. The major contribution to the decay comes from shorter components ($\tau_f \approx 0.67$ ns, 75% and $\tau_f \approx 3.0$ ns, 17%), which can be attributed to distinct aggregated species such as dimers or higher order nonspecific aggregates.[30]

Thus, it is expected that these differences in the two porphyrinoids will contribute to a different combination of interactions with GO: $\pi-\pi$ interactions will be present in both cases, but electrostatic repulsions between AlPcS4 and GO will take place in opposition to attractive electrostatic interactions for MM-PLL with GO.

Upon addition of increasing amounts of dispersed GO, there are subtle changes in the UV/Vis absorption of the porphyrin, Figure 5A: a 2 nm redshift from 418 to 420 nm and broadening of the Soret band. Using the spectrum of free MM-PLL (with the same concentration) as a reference, a trough appears at 419 nm which becomes deeper as the concentration of GO is increased, meaning that less and less free porphyrin is available; together with the growth of a new redshifted absorption

peak at 435 nm (inset Figure 5A). These findings are in agreement with $\pi-\pi$ interactions between the porphyrin and GO.[31] Due to the strong absorption of the PLL chains attached to the porphyrins, which superimposes that of the GO (characteristic peak at 231 nm in water), we may not infer whether there were any changes in the electronic structure of GO upon interaction with MM-PLL. In the case of the phthalocyanine, there are no significant changes on the UV/Vis spectra obtained at increasing amounts of GO, Figure 5B. Again, by using the spectrum of the free phthalocyanine in water we see that, in this case, no additional peaks are observed and the difference matches quite well the spectrum of GO alone (inset Figure 5B), thus suggesting that no changes in the electronic structure of GO took place. In this case, electrostatic repulsions may prevent GO and AlPcS4 to attain a suitable distance for $\pi-\pi$ interactions to occur. The interaction of other negatively charged π-systems was reported with chemically reduced GO. This was suggested to be possible due to a relative electrically neutral interior of the reduced graphene sheets, different from GO, with negatively charged carboxylic groups present only on the edges of the sheets.[32]

The fluorescence of both porphyrinoids in water is differently affected by the addition of GO. These measurements were performed with matching absorbances of the porphyrinoid at the excitation wavelength. The typical band at 682 nm of AlPcS4 is almost unaltered up to an addition of 0.014 mg mL^{-1} of GO, Figure 5D. By contrast, in the case of MM-PLL the intensity of the two typical emission bands (Q(0,0) at 653 nm and Q(0,1) at 719 nm) is greatly diminished upon addition of increasing amounts of GO, Figure 5C. No new bands are detected pointing out that any possible complex or aggregate formed is nonfluorescent or has a much lower fluorescence quantum yield than that of the dye. This fluorescence quenching can be assigned to electron or energy transfer. GO itself has been reported to show emission whose intensity depended on the solution pH and ionic strength,[33] and its fluorescence has been used for cellular imaging and drug delivery.[34] Earlier studies suggested that the GO photoluminescence originates from the radiative recombination of electron-hole pairs generated in sp^2 clusters with time constants ranging from femto- to picoseconds.[35] In view of atomic structure, the GO emission is predominantly from the electron transitions between the less oxidized region (−C=C−) and the boundary of oxidized region (C−O, C=O and O=C−OH).[36]

We have confirmed that due to its expected low intensity at neutral pH, the intrinsic fluores-
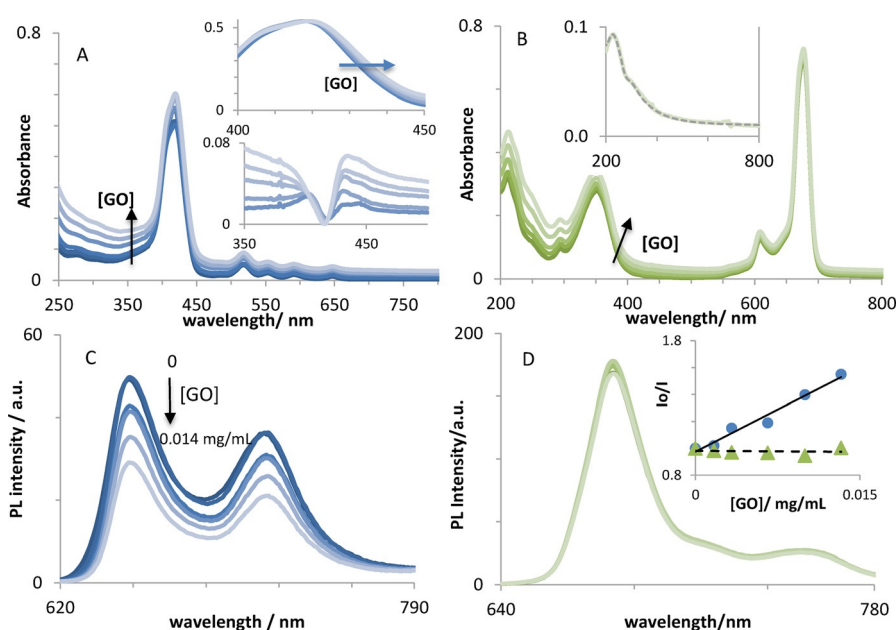
Figure 5. UV/Vis absorption (A and B) and fluorescence (C and D) spectra of MM-PLL/GO (blue color) and of AlPcS4/GO (green color) aqueous suspensions. Insets (A, B): see text for explanation. Inset (D) Stern–Volmer plot of intensity quenching (blue dots: MM-PLL; green triangles: AlPcS4). [Porphyrinoid] = 5 μM; λ_{exc} = 405 nm.

cence of GO does not interfere with the emission of the porphyrinoids under the conditions used.

Stern–Volmer plots representing the dependence of the fluorescence intensities ratio (accounted by the area under each fluorescence spectrum) in the absence (I_0) and in the presence (I) of GO on the concentration of the latter, show a linear dependence in the case of MM-PLL, inset Figure 5 D. Steady-state fluorescence contains the contribution of both static and dynamic quenching mechanisms. The determination of fluorescence lifetimes of the fluorophore is the most definitive method for distinguishing between the two types of quenching. In the case of the dynamic quenching, the fluorophore lifetime decreases with the increase

Figure 6. UV/Vis absorption (A and B) and photoluminescence (C and D) spectra of MM-PLL/AuNP@GO (blue color) and of AlPcS4/AuNP@GO (green color) hybrid aqueous suspensions. Inset (D) Stern–Volmer plot of intensity quenching (blue dots: MM-PLL; green triangles: AlPcS4). [Porphyrinoid] = 5 μm; λ_{exc} = 405 nm.

of the quencher concentration. In the present study, the fluorescence lifetime of AlPcS4 remains monoexponential and unchanged (τ_f = 4.90 ns), as expected. In the case of MM-PLL, the complex three-exponential decay is not significantly altered upon addition of GO (data not shown). Therefore, the contribution of dynamic quenching is not significant. The major contribution for the quenching process must then come from static effects. Their origin is related to the formation of a nonfluorescent complex/aggregate considering the changes observed in the absorption spectra. Under such conditions, the fluorescence lifetime is not expected to change since the fluorophore (which is not complexed/aggregated) is able to emit in its normal way. However, a decrease in the fluorescence intensity of the sample is expected to occur upon each increase of the quencher concentration since there will be less and less free fluorophore to emit due to complexation. A similar behavior had already been reported for the interaction of the cationic rhodamine 101 with GO in aqueous solution.[37]

It is clear that the quenching is only effective for the porphyrin since a flat line is obtained in the case of AlPcS4 denoting the absence of quenching by GO. This behavior reflects the importance of favorable electrostatic attractions in promoting porphyrinoid/GO interactions: unfavorable electrostatic repulsions existent in AlPcS4/GO system weakens such interactions.

Interactions between AuNP@GO and porphyrinoids

In the next stage, gold nanoparticles were grown on the surface of GO and the interactions of these hybrids with porphyrinoids in water were followed. Absorption spectra obtained at increasing concentrations of the AuNP/GO hybrid show a concomitant increase of the signal in the region corresponding to
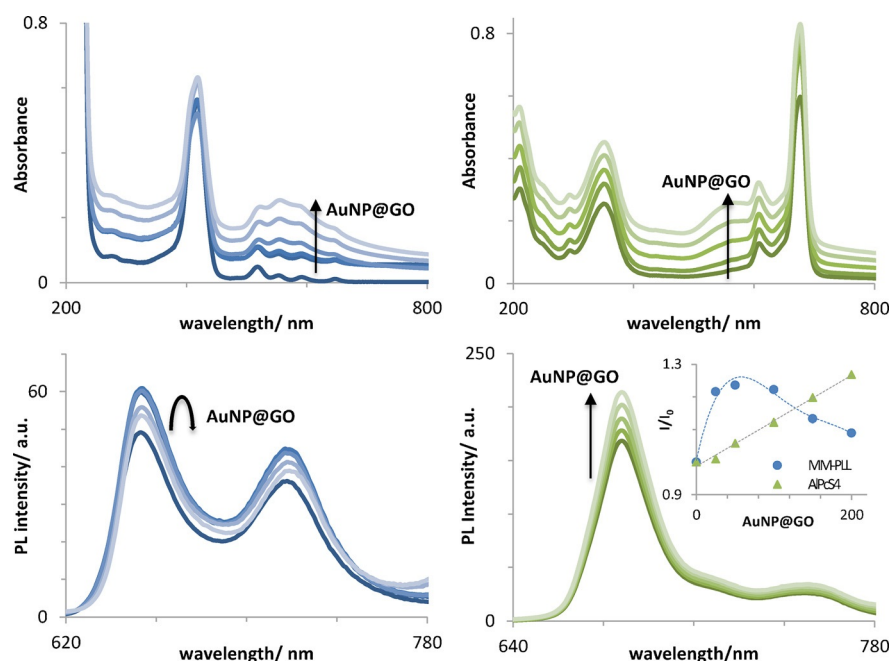
the SPRB of AuNP, but no other significant changes were detected for either porphyrinoids, Figure 6 A and 6 B. Regarding the spectrum of AuNP@GO, a comparison with that obtained by difference of porphyrinoid with and without AuNP@GO shows that there is broadening and redshift ($\approx$ 20 nm) of the SPRB of AuNP, which can be due to interparticle interactions induced by the porphyrinoids. On the other hand, the fluorescence spectra showed distinct behavior for the two molecules. In the case of the porphyrin, Figure 6 C, a strong increase of the intensity upon addition of the hybrid takes place followed by a decrease as further amount is added; whereas in the case of the phthalocyanine a steady increase of the signal follows the addition of AuNP@GO, Figure 6 D. A maximum of 30 % increase was obtained for each porphyrinoid (inset Figure 6 D).

To clarify if a similar effect can be obtained just in presence of AuNP without GO, we added increasing amounts of preformed AuNP (TEM image of these AuNP can be found in Figure S6, Supporting Information) and followed the porphyrinoid fluorescence, Figure 7. Although in both cases it was possible to detect an increase of the fluorescence signal—about 5 % in the case of MM-PLL and 11 % in the case of AlPcS4—this was clearly less effective than in presence of the hybrid.

An intrinsic low emission with maximum at 617 nm was reported for AuNP (and some nanoclusters) with diameters of approximately 15 nm synthetized using the standard citrate reduction method.[38] However, in our case a test to the hybrid with and without the porphyrinoid made under the same experimental conditions did not show any contamination from the hybrid photoluminescence. Such a result is somehow expected taking into account that AuNP are essentially located on the GO surface and that the latter can effectively quench Au photoluminescence.[39] Therefore, the fluorescence detected
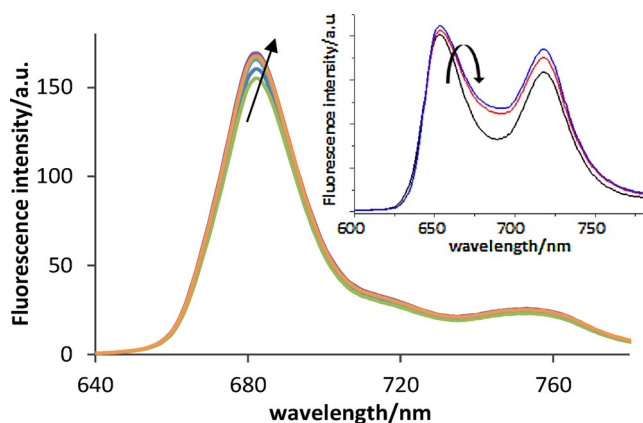
Figure 7. Fluorescence spectra of AlPcS4 (inset: MM-PLL) in the presence of increasing amounts of preformed AuNP in aqueous solution.

comes solely from the respective porphyrinoid and in both cases there is an enhancement dependent on the amount of added hybrid.

The phenomenon of fluorescence enhancement promoted by a metal surface (MEF) has been known for some time and will affect both radiative and nonradiative decay rates. To that matter, fluorescence decays were obtained in solution and showed a notorious decrease of average lifetimes of both fluorophores in the presence of the AuNP@GO (Table S1, Supporting Information). For MEF to occur, the fluorophore needs to be close enough to the plasmonic nanostructure, since the field enhancement decays nearly exponentially with distance from the metallic surface. If the fluorophore is closer than 5 nm to the surface, its fluorescence will be quenched significantly due to the nonradiative decay through energy and/or charge transfer to the metal.[40] The strong interactions MM-PLL/GO are due to promote a closer contact with the hybrid and therefore, at higher amounts of the latter the average distances porphyrinoid–hybrid are shorter so that fluorescence quenching surpasses the enhancement. As for AlPcS4 there is not a significant interaction with GO and the distances Pc–hybrid remain larger thus allowing the enhancement by AuNP to prevail. A study involving thin films of a porphyrin and AuNP showed that the latter quenched the porphyrin's fluorescence very effectively mainly via an energy-transfer process with an estimated critical distance of 6.4 nm.[41] It is important to point out that in the case of a self-assembled system in which both NP and porphyrinoid entities do not have a rigid location, NP distribution is expected to affect their interaction and thus, the porphyrinoid fluorescence intensity. Nonetheless, a good reproducibility of the SV plots was always obtained. To this contributes the high density of oxygen-containing groups on GO surface and the confirmation that this in-situ method leads to AuNP location solely on GO sheets.

In the next stage, we studied and compared fluorescence signals from deposited samples containing porphyrinoids alone, in presence of GO and of AuNP@GO, using FLIM.

FLIM images of deposited samples

We started by testing GO and AuNP@GO for a possible interference in the background signal of the samples with porphyrinoids. None of the materials had a detectable signal under the experimental conditions, which is adequate to follow the porphyrinoids' fluorescence.

The deposition of the porphyrinoids showed a heterogeneous image in the case of MM-PLL, Figure 8 A, which is consis-
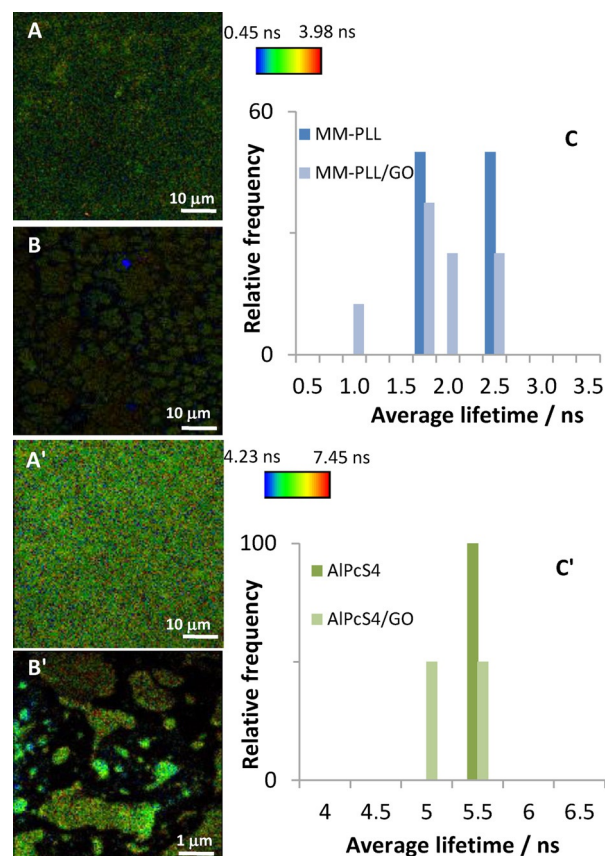
Figure 8. FLIM images (A, A′, B, B′) and average fluorescence lifetime distribution (C, C′) obtained from decay analysis of about 20 point measurements of MM-PLL (top) and AlPcS4 (bottom) free and associated to GO.

tent with some aggregation of the porphyrin upon deposition on glass, similar to what already happened in aqueous solution. As expected, the average lifetimes are shorter than the typical values obtained for monomeric porphyrins in solvents.

In the presence of GO, Figure 8 B, it is possible to distinguish flake-like regions in agreement to those already visualized by TEM, which correspond to GO sheets covered with porphyrin. The fluorescence lifetimes associated to the images display a broader distribution due to some competition between porphyrin-GO interactions and π–π stacking of porphyrins on the surface of the carbon material, Figure 8 C. Due to the heterogeneity of the deposited system it is not possible to make a quantitative study of the fluorescence signal dependence on the concentration of GO. Nonetheless, there is a clear decrease of the fluorescence intensity with the increase of [GO] (Figure S7, Supporting Information).

In the case of AlPcS4 alone, we obtained a nearly uniform image with a fluorescence lifetime similar to that of the phthalocyanine in aqueous solution. However, in the presence of GO some heterogeneity is depicted: GO flakes with dimensions of a few to tens of microns stand out from the noninterfering background. Thus, AlPcS4 is also covering GO flakes and a slight shortening of lifetimes is thus obtained. However, no dependence on [GO] can be detected in this case.

We followed the porphyrinoids' fluorescence upon interaction with the hybrid Au@GO in deposited samples. FLIM images obtained for the porphyrin show distinct regions, Figure 9 A: short-lived round entities spread through, and some

The heterogeneity depicted in the image points to some roughness of the deposited sample, which can lead to differences in fluorophore–hybrid interdistances and relative orientations. The latter will thus contribute to the broadening of the lifetime distribution, Figure 9 D.

This data reinforces the role of porphyrinoid–GO interactions in controlling the fluorescence sensitivity of the dye to the metal vicinity: the preponderance of porphyrin-GO interactions lead to fluorescence quenching whereas MEF prevails for the noninteracting AlPcS4. Further studies are still required to fully understand the underlying mechanism of the fluorescence quenching phenomena.

Figure 9. (A,B) FLIM images and (C,D) normalized lifetime histograms of porphyrinoids (MM-PLL, top; AlPcS4, bottom) free and interacting with the hybrid AuNP@GO deposited on a glass surface. Inset of B: emission intensity image.

long-lived micrometric regions. Accordingly, the histogram shows a broader distribution of average fluorescence lifetimes as compared to that for the porphyrin alone which is shifted to shorter values in presence of the hybrid. This behavior points in one hand to some de-aggregation of the porphyrin due to interactions with the hybrid, therefore there is a slight increase from the contribution of longer lifetimes. On the other hand, the strong interaction of porphyrin monomers with GO and with the hybrid will lead to fluorescence quenching which increases the contribution from short lifetimes, Figure 9 C.

In the case of the AlPcS4, we also have a distinct behavior relative to water. The narrow average lifetime distribution obtained for the phthalocyanine alone changes to a broad distribution associated to a more heterogeneous image, Figure 9 D. It is possible to distinguish round spots with sizes within the diffraction-limit resolution (ca. 350 nm), Figure 9 B, with short lifetimes and with a higher intensity than its surroundings, inset Figure 9 B, pointing out the enhancing effect of AuNP@GO.

Conclusions

We have prepared and characterized a hybrid material constituted of graphene oxide and gold nanoparticles and studied its interaction with different porphyrinoids. Based on optical absorption and fluorescence results there is no evidence for ground-state nor singlet excited-state interactions between the negatively charged AlPcS4 and GO in solution. In the case of MM-PLL, the long amino-rich polylysine chain promotes the interaction with the oxygen groups of GO in detriment of porphyrin aggregation detected for the free molecule in water. The efficient quenching of the porphyrin characteristic emission in the composite suggests that electrons are transported from the excited MM-PLL to GO sheets.

By contrast, in presence of the AuNP@GO hybrid there is an enhancement of the dyes' fluorescence in solution. In the case of AlPcS4 there is a concomitant increase of the fluorescence intensity with the addition of the hybrid whereas in the case of MM-PLL there is an optimal amount of hybrid above which the signal reverses and a quenching effect prevails. The fluorescence intensity of the dyes could also be detected in films by FLIM. The enhancement in intensity was followed by a strong decrease in the average fluorescence lifetime of both porphyrinoids. A broad lifetime distribution was obtained which could be explained in terms of a distribution of plasmon resonance effects due to distinct porphyrinoid- AuNP distances promoted by the heterogeneity of the deposited sample. Our findings are expected to be useful as a general methodology for constructing multicomponent graphene-based nanohybrids with potential applications in energy conversion and sensing.

Experimental Section

Synthesis of GO

In order to obtain graphene oxide, we used a variation of the Hummers method.[42] Briefly, 1 g of graphite powder (synthetic, conducting grade, −325 mesh, 99.9995 % metals basis, Alfa Aesar) was suspended in 23 mL of H_2SO_4 concentrated and stirred for 12 h. The suspension was brought to 0 °C and 3 g of $KMnO_4$ was gradually added. After the addition, sonication for 6 h was performed and afterwards 46 mL of H_2O was slowly added and left to boil for 30 min. To terminate the reaction, a solution of H_2O_2 30 % in water was added. The final product was separated by centrifugation and washed with 5 % HCl and water.

Synthesis of AuNP@GO

AuNP@GO was prepared using a method developed by Kamat et al.[23] with some variations. NaAuCl$_4$·2H$_2$O (99%, Sigma–Aldrich) ≈1 mm, was dissolved in 2% TEG (Fluka) solutions and added to 2 mg of the GO prepared before. The suspension was submitted to sonication for 4 h. The possible AuNP left in solution were removed by centrifugation cycles at 3000 rpm for 20 min.

Sample preparation

Aqueous dispersions of exfoliated GO were obtained by ultrasonication during 1 h. Porphyrinoid–GO complexes were prepared for absorption and fluorescence measurements by mixing a minute amount (less than 25 μL) of a DMSO stock solution in the case of the MM-PLL (synthesized by us, see Supporting Information for details) and of an aqueous stock solution in the case of AlPcS4 (99%, Porphyrin Products) with different amounts of GO aqueous stock solution. The solution in each flask was then diluted to 5 mL by bidistilled water (final porphyrinoid concentration 5 μm). Immobilized samples for FLIM were prepared on previously cleaned and hydrophilized glass slides (30 min in freshly prepared piranha solution, H$_2$O$_2$:H$_2$SO$_4$ = 1:3) by drop-casting.

Characterization

The experimental zeta potential values (ζ) of GO aqueous suspensions were determined in a Doppler electrophoretic light scattering analyzer, Zetasizer Nano ZS from Malvern Instruments Ltd. A PerkinElmer spectrophotometer Lambda 35 was employed in UV/Vis extinction measurements. Steady-state fluorescence spectra were obtained with a SPEX® Fluorolog spectrofluorimeter (HORIBA Jobin Yvon) in a FL3–11 configuration. The instrumental response was corrected by means of a correction function provided by the manufacturer. Fluorescence lifetimes were obtained with a time-correlated single-photon counting (TC-SPC) technique using commercial equipment Microtime 200 (PicoQuant, Berlin, Germany). Excitation was achieved using pulsed laser diode heads (405 nm; 638 nm), with varied repetition rate (10, 20 or 40 MHz). Appropriate bandpass filters (600–800 nm transmission band for the blue-diode laser and the 695AF55 filter for the red-diode laser) were used to eliminate backscattered light in the photomultiplier tube from PicoQuant (model PMA-182). Data analysis was performed by a deconvolution method using a nonlinear least-squares fitting program, based on the Marquardt algorithm. The goodness of the fit was evaluated by the usual statistical criteria and by visual inspection of the weighted residuals distribution and the autocorrelation function. FLIM was performed in the same set-up and a more detailed description can be found elsewhere.[43] Briefly, the 638 nm pulsed diode laser was focused by a water immersion objective (60x; 1.2 NA) into the sample. Fluorescence was collected by the same microscope objective, passed through the dichroic mirror and suitable band pass filter, focused through a pinhole (30 μm), to reject out-of-focus light, onto a single-photon counting avalanche photodiode (PerkinElmer) whose signal was processed by a TimeHarp 200 TC-SPC PC-board (PicoQuant) working in the special Time-Tagged Time-Resolved mode which stores all relevant information for every detected photon. The average photon count rate was 0.5–1×10^4 counts s^{-1}.

TEM images were obtained with a Hitachi H-8100 electron microscope operated at 200 kV. A drop of sample solution was deposited and air dried in a carbon/Formvar-coated copper grid. Tapping mode AFM was performed on a Multimode AFM instrument with Nanoscope IIIa controller from Digital Instruments. Si cantilevers with a spring constant of 42 N m^{-1} and a resonance frequency of ≈300 kHz were employed for imaging. Mica substrates purchased from Veeco were cleaved immediately before sample deposition. To remove excess solution from the substrate surface after a specific time (20 min), a N$_2$ flux was used.

[1] A. K. Geim, K. S. Novoselov, *Nat. Mater.* **2007**, *6*, 183–191.
[2] a) Q. H. Wang, M. C. Hersam, *Nat. Chem.* **2009**, *1*, 206–211; b) T. Kuila, S. Bose, A. K. Mishra, P. Khanra, N. H. Kim, J. H. Lee, *Prog. Mater. Sci.* **2012**, *57*, 1061–1105; c) B. F. Machado, P. Serp, *Catal. Sci. Technol.* **2012**, *2*, 54–75; d) F. Bonaccorso, L. Colombo, G. Yu, M. Stoller, V. Tozzini, A. C. Ferrari, R. S. Ruoff, V. Pellegrini, *Science* **2015**, *347*, 1246501.
[3] a) Y. T. Liang, B. K. Vijayan, K. A. Gray, M. C. Hersam, *Nano Lett.* **2011**, *11*, 2865–2870; b) S. Morales-Torres, L. M. Pastrana-Martinez, J. L. Figueiredo, J. L. Faria, A. M. T. Silva, *Environ. Sci. Pollut. Res. Int.* **2012**, *19*, 3676–3687; c) V. Georgakilas, M. Otyepka, A. B. Bourlinos, V. Chandra, N. Kim, K. C. Kemp, P. Hobza, R. Zboril, K. S. Kim, *Chem. Rev.* **2012**, *112*, 6156–6214; d) W. Wei, X. Qu, *Small* **2012**, *8*, 2138; e) L. Rodríguez-Pérez, M. A. Herranz, N. Martín, *Chem. Commun.* **2013**, *49*, 3721–3735.
[4] a) Q. Su, S. Pang, V. Alijani, C. Li, X. Feng, K. Müllen, *Adv. Mater.* **2009**, *21*, 3191–3195; b) B. Martín-García, M. M. Velázquez, F. Rossella, V. Bellani, E. Diez, J. L. G. Fierro, J. A. Pérez-Hernández, J. Hernández-Toro, S. Claramunt, A. Cirera, *ChemPhysChem* **2012**, *13*, 3682–3690.
[5] a) N. Karousis, J. Ortiz, K. Ohkubo, T. Hasobe, S. Fukuzumi, A. Sastre-Santos, N. Tagmatarchis, *J. Phys. Chem. C* **2012**, *116*, 20564–20573; b) T. Skaltsas, S. Pispas, N. Tagmatarchis, *Chem. Eur. J.* **2013**, *19*, 9286–9290; c) J. Malig, N. Jux, D. M. Guldi, *Acc. Chem. Res.* **2013**, *46*, 53–64.
[6] a) P. V. Kamat, *J. Phys. Chem. Lett.* **2010**, *1*, 520–527; b) P. T. Yin, S. Shah, M. Chhowalla, K.-B. Lee, *Chem. Rev.* **2015**, *115*, 2483–2531.
[7] a) G. Gonçalves, P. A. A. P. Marques, C. M. Granadeiro, H. I. S. Nogueira, M. K. Singh, J. Grácio, *Chem. Mater.* **2009**, *21*, 4796–4802; b) Y. H. Lee, L. Polavarapu, N. Gao, P. Yuan, Q.-H. Xu, *Langmuir* **2012**, *28*, 321–326; c) I. V. Lightcap, S. Murphy, T. Schumer, P. V. Kamat, *J. Phys. Chem. Lett.* **2012**, *3*, 1453–1458.
[8] a) X. Huang, I. H. El-Sayed, W. Qian, M. A. El-Sayed, *J. Am. Chem. Soc.* **2006**, *128*, 2115–2120; b) P. V. Kamat, *J. Phys. Chem. C* **2007**, *111*, 2834–2860; c) C. J. Bueno-Alejo, M. Grenier, J. C. Netto-Ferreira, J. C. Scaiano, *Org. Lett.* **2011**, *13*, 204–207.
[9] a) K. Aslan, J. R. Lakowicz, C. D. Geddes, *Curr. Opin. Chem. Biol.* **2005**, *9*, 538–544; b) P. K. Jain, X. Huang, I. H. El-Sayed, M. A. El-Sayed, *Plasmonics* **2007**, *2*, 107–118; c) N. L. Pacioni, M. Gozáles-Béjar, E. Alarcón, K. L. McGilvray, J. C. Scaiano, *J. Am. Chem. Soc.* **2010**, *132*, 6298–6299; d) Q. Cui, F. He, L. Li, H. Möhwald, *Adv. Colloid Interface Sci.* **2014**, *207*, 164–177.
[10] J. Zhang, Y. Fu, M. H. Chowdhury, J. R. Lakowicz, *J. Phys. Chem. C* **2008**, *112*, 18–26.
[11] a) K. Ray, R. Badugu, J. R. Lakowicz, *Chem. Mater.* **2007**, *19*, 5902–5909; b) L. Lu, Y. X. Qian, L. H. Wang, K. K. Ma, Y. D. Zhang, *ACS Appl. Mater. In-*

terfaces **2014**, *6*, 1944–1950; c) T. Labouret, J.-F. Audibert, R. b. Pansu, B. Palpant, *Small* **2015**, 11, 4475–4479.

[12] Y. Chen, K. Munechika, D. S. Ginger, *Nano Lett.* **2007**, *7*, 690–696.

[13] S. Vukovic, S. Corni, B. Mennucci, *J. Phys. Chem. C* **2009**, *113*, 121–133.

[14] a) J. Geng, B.-S. Kong, H.-T. Jung, *Chem. Commun.* **2010**, *46*, 5091–5093; b) A. Wojcik, P. V. Kamat, *ACS Nano* **2010**, *4*, 6697–6706; c) J. Kim, L. J. Cote, F. Kim, J. Huang, *J. Am. Chem. Soc.* **2010**, *132*, 260–267; d) W. W. Tu, J. P. Lei, S. Y. Zhang, H. X. Ju, *Chem. Eur. J.* **2010**, *16*, 10771–10777; e) L. Wibmer, L. M. O. Lourenço, A. Roth, G. Katsukis, M. G. P. M. S. Neves, J. A. S. Cavaleiro, J. P. C. Tomé, T. Torres, D. M. Guldi, *Nanoscale* **2015**, *7*, 5674–5682; f) S. P. Economopoulos, N. Tagmatarchis, *J. Phys. Chem. C* **2015**, *119*, 8046–8053.

[15] a) T. Tachikawa, S.-C. Cui, M. Fujitsuka, T. Majima, *Phys. Chem. Chem. Phys.* **2012**, *14*, 4244–4249; b) M. Supur, Y. Kawashima, K. Mase, K. Ohkubo, T. Hasobe, S. Fukuzumi, *J. Phys. Chem. C* **2015**, *119*, 13488–13495.

[16] a) H. Li, S. Liu, J. Tian, L. Wang, W. Lu, Y. Luo, A. M. Asiri, A. O. Al-Youbi, X. Sun, *ChemCatChem* **2012**, *4*, 1079–1083; b) P. Xing, L. Bai, H. Chen, P. H. Tham, A. Hao, Y. Zhao, *ChemNanoMat* **2015**, DOI: 10.1002/cnma.201500095.

[17] a) D. Wang, L. Chen, *Nano Lett.* **2007**, *7*, 1480–1484; b) S. M. Andrade, P. Raja, V. K. Saini, A. S. Viana, P. Serp, S. M. B. Costa, *ChemPhysChem* **2012**, *13*, 3622–3631.

[18] C. A. T. Laia, S. M. B. Costa, *J. Phys. Chem. B* **2008**, *112*, 4276–4282.

[19] R. Teixeira, P. M. R. Paulo, A. S. Viana, S. M. B. Costa, *J. Phys. Chem. C* **2011**, *115*, 24674–24680.

[20] L. Li, J.-Y. m. Chen, X. Wu, P.-N. Wang, Q. Peng, *J. Phys. Chem. B* **2010**, *114*, 17194–17200.

[21] a) J. W. Borst, A. J. W. G. Visser, *Meas. Sci. Technol.* **2010**, *21*, 102002; b) K. Suhling, L. M. Hirvonen, J. A. Levitt, P.-H. Chung, C. Tregidgo, A. Le Marois, D. A. Rusakov, K. Zheng, S. Ameer-Beg, S. Poland, S. Coelho, R. Hendersone, N. Krstajic, *Med. Photon.* **2015**, *27*, 3–40.

[22] C. Gómez-Navarro, R. T. Weitz, A. M. Bittner, M. Scolari, A. Mews, M. Burghard, K. Kern, *Nano Lett.* **2007**, *7*, 3499–3503.

[23] K. Vinodgopal, B. Neppolian, I. V. Lightcap, F. Grieser, M. Ashokkumar, P. V. Kamat, *J. Phys. Chem. Lett.* **2010**, *1*, 1987–1993.

[24] M.-K. Chuang, F.-C. Chen, C.-S. Hsu, *J. Nanomater.* **2014**, *2014*, 736879.

[25] S. Link, M. A. El-Sayed, *J. Phys. Chem. B* **1999**, *103*, 4212–4217.

[26] W. S. Rasband, ImageJ, U.S. National Institutes of Health, Bethesda, Maryland, USA, http://imagej.nih.gov/ij/, July 2014.

[27] a) S. M. Andrade, S. M. B. Costa, *Chem. Eur. J.* **2006**, *12*, 1046–1057; b) S. M. Andrade, C. Teixeira, D. M. Togashi, A. J. F. N. Sobral, S. M. B. Costa, *J. Photochem. Photobiol. A* **2006**, *178*, 225–235.

[28] M. Kasha, *Radiat. Res.* **1963**, *20*, 55–70.

[29] R. Teixeira, S. M. Andrade, V. V. Serra, P. M. R. Paulo, A. Sánchez-Coronilla, M. G. P. M. S. Neves, J. A. S. Cavaleiro, S. M. B. Costa, *J. Phys. Chem. B* **2012**, *116*, 2396–2404.

[30] a) S. M. Andrade, R. Teixeira, S. M. B. Costa, A. J. F. N. Sobral, *Biophys. Chem.* **2008**, *133*, 1–10; b) S. M. Andrade, S. M. B. Costa, J. W. Borst, A. van Hoek, A. J. W. G. Visser, *J. Fluoresc.* **2008**, *18*, 601–610.

[31] J. Geng, H.-T. Jung, *J. Phys. Chem. C* **2010**, *114*, 8227–8234.

[32] S. Liu, J. Tian, L. Wang, H. Li, Y. Zhang, X. Sun, *Macromolecules* **2010**, *43*, 10078–10083.

[33] a) C. Galande, A. D. Mohite, A. V. Naumov, W. Gao, L. Ci, A. Ajayan, H. Gao, A. Srivastava, R. Bruce Weisman, P. M. Ajayan, *Sci. Rep.* **2011**, *1*, 85; b) J.-L. Chen, X.-P. Yan, *Chem. Commun.* **2011**, *47*, 3135–3137.

[34] a) X. Sun, Z. Liu, K. Welsher, J. T. Robinson, A. Goodwin, S. Zaric, H. Dai, *Nano Res.* **2008**, *1*, 203–212; b) J. Peng, W. Gao, B. K. Gupta, Z. Liu, R. Romero-Aburto, L. Ge, L. Song, L. B. Alemany, X. Zhan, G. Gao, S. A. Vithayathil, B. A. Kaipparettu, A. Marti, T. Hayashi, J.-J. Zhu, P. M. Ajayan, *Nano Lett.* **2012**, *12*, 844–849; c) E. Morales-Narváez, A. Merkoçi, *Adv. Mater.* **2012**, *24*, 3298–3308.

[35] S. Kaniyankandy, S. N. Achary, S. Rawalekar, H. N. Ghosh, *J. Phys. Chem. C* **2011**, *115*, 19110–19116.

[36] J. Shang, L. Ma, J. Li, W. Ai, T. Yu, G. G. Gurzadyan, *Sci. Rep.* **2012**, *2*, 792.

[37] E. Bozkurt, M. Acar, Y. Onganer, K. Meral, *Phys. Chem. Chem. Phys.* **2014**, *16*, 18276–18281.

[38] a) J. Zheng, C. Zhang, R. M. Dickson, *Phys. Rev. Lett.* **2004**, *93*, 077402; b) S. Roy, C. K. Dixit, R. Woolley, R. O'Kennedy, C. McDonagh, *Langmuir* **2011**, *27*, 10421–10428.

[39] M. C. Dalfovo, G. I. Lacconi, M. Moreno, M. C. Yappert, G. U. Sumanasekera, R. C. Salvarezza, F. J. Ibanez, *ACS Appl. Mater. Interfaces* **2014**, *6*, 6384–6391.

[40] T. Ming, H. Chen, R. Jiang, Q. Li, J. Wang, *J. Phys. Chem. Lett.* **2012**, *3*, 191–202.

[41] A. Kotiaho, R. Lahtinen, H. Lehtivuori, N. V. Tkachenko, H. Lemmetyinen, *J. Phys. Chem. C* **2008**, *112*, 10316–10322.

[42] W. S. Hummers, R. E. Offeman, *J. Am. Chem. Soc.* **1958**, *80*, 1339–1339.

[43] V. V. Serra, S. M. Andrade, M. G. P. M. S. Neves, J. A. S. Cavaleiro, S. M. B. Costa, *New J. Chem.* **2010**, *34*, 2757–2765.